AN INVESTIGATION OF TURBULENT FLOW IN NON-RETURN DISC VALVES

H. A. Abdalla, B. A. Khalifa, A. S. Huzayyin
A. R. Dyab and S. N. Abdu

Department of Mechanical Power Engineering, Faculty of Engineering,
Minufiya University, Shebin El-Kom, Egypt.

ABSTRACT

In this paper, computational and experimental studies are reported on a steady incompressible flow through disc valves. The numerical procedure used for this purpose solves the governing equations using the SIMPLE algorithm. The time-averaged governing equations are closed using the k-ε turbulence model. The predicted results are compared with the experimental results. The effects of the thickness of the valve disc, the disc overlap length and valve openings on the valve characteristics and the turbulent flow structure are studied. The predicted flowfield parameters indicate that, the flow velocity and direction are changed as it approaches the valve disc because of the decreasing flow area and the valve disc opening. The flow is accelerated as it passes between the seat and the disc, the flow direction is toward the periphery of the disc. A separated flow region is formed downstream the valve seat. Near the periphery of the disc, the flow separates and becomes a jet flow which is bounded on one side by the wall and on the other side by the recirculated flow region in the wake of the valve disc. The jet and recirculated flows interact, mix and recompress downstream. The flow characteristics of the disc valves are strongly affected by the interaction between the jet and recirculation flows downstream of the valve disc. The size and structure of the separated and recirculated flows regions depend on the valve geometry and the valve disc opening. Qualitative agreement between predicted and measured results was obtained.

Keywords: Disc valves, Valve characteristics, Valve geometry, Valve performance, Separated flow.

INTRODUCTION

Seating valves such as poppet and disc valves are commonly used in fluid power applications. They offer a number of advantages over spool valves, in that they can provide a positive seal and do not require very fine machining tolerances. Seating valves are widely used in a variety of applications in which their low flow resistance and robustness make them ideal. Examples include internal combustion engine and reciprocating piston pump porting valves and pressure control valves, such as relief valves and non-return valves. A great deal of research has been published on the flow characteristics of hydraulic valves. This serves to indicate that valve flow can be a highly complex process which is strongly dependent on the details of the valve geometry, the fluid properties and the operating conditions. Separating and reattachment of jets can have a profound effect on the flow, pressure and force characteristics as well as influencing the susceptibility to cavitation. Although many researchers have published results of experimental work on the steady state characteristics of poppet and disc valves, the understanding of their operation is still rather limited. Experimental work on valve flow stretches back over many years and the extent is quite comprehensive. Schrenk [1] published results of experimental work on a wide variety of poppet and disc valves. His

work was concentrated on the pressure-flow characteristics with very little details on the force characteristics. Stone [2] studied the characteristics of hydraulic poppet valves with sharp-edged seats. However, the work was limited to relatively small openings and low Reynolds number. His results showed that the flow forces are strongly influenced by the downstream configuration. The smaller diameter of the downstream chamber gives higher forces. He also concluded that the results were limited in accuracy and scope, and that further work was necessary to be done. Oki and co-workers [3-5] published several papers regarding an experimental work on disc valves, but most of this work was concentrated on water jets discharging into air. They used a relatively narrow ring-shaped seat which is common with nozzle-flapper valves. However, disc valves used in reciprocating pumps and compressors commonly have large flat seats, [6], and this design was recently chosen for the experiments reported by Johnston, *et. al.* [7]. The results of measured flow coefficients and force characteristics showed marked differences depending on valve geometry and its opening. These differences were explained with reference to visualized flow patterns.

Several attempts have been made to model the flow through disc or flapper valves analytically. Takenaka *et. al.* [8] and Hagiwara [9] attempted to solve the Navier-Stokes equations for the flow between the disc and valve seat. They neglected the effects of flow separation. Thus, their prediction did not correlate well with their experimental measurements, particularly at larger openings where the flow separation has a greater effect. The more recent development of computational fluid dynamics techniques provides a great scope for the study of valve flow. Thus the early attempts were aimed at simulating flow in spool valves or in disc valves that could be simply defined. Hayashi *et. al.* [10] simulated the flow in nozzle-flapper valves. Their results showed jet separation and reattachment and compared well with experimental results. Jet reattachment in turbulent flow is a much more difficult phenomenon to predict. Pountney *et. al.* [11] performed a study of the turbulent flow through spool valves orifices. No comparison was made with experimental results in their work and some favourable comparisons were made with potential flow analysis. Considerable research was carried out recently on the simulation of fluid flow in poppet valves by Vaughan *et. al.* [12]. They performed a computational study of fluid flow through poppet valves using a finite volume computational fluid dynamics program. Simulation were compared with experimental measurements and visualized flow patterns. Qualitative agreement between simulated and visualized flow patterns was good. Hu and Hsu [13] investigated the turbulent flowfield downstream of a partly opened throttle valve of a motorcycle carburettor to which a section of straight pipe is attached to model the inlet pipe. They found that the flow downstream of the partly opened throttling valve is composed of a recirculation region, a three-dimensional jet stream and a small boundary layer. This study clearly demonstrates that the jet stream, which includes a major portion of the flow going downstream, shows similarity of axial velocity profiles on planes normal to the angular direction. Interesting jet and boundary layer flow interactions are also reported in this study.

The work presented in this paper aimed to study the steady-state flow characteristics and performance of hydraulic disc valves which are used in hydraulic piping systems working with water-based fluids. Simulations of flow through non-return valves (disc valves) were performed using a finite volume computational fluid dynamics techniques. An experimental study was conducted and the obtained experimental results were compared with the computational results. The effect of a range of basic changes to the geometry of disc valves was studied. These changes showed some interesting effects on the characteristics of such valves.

MATHEMATICAL MODEL AND CALCULATION METHOD

The mathematical model employed to obtain the flow predictions and to solve numerically the governing equations for the

averaged values of the components of the velocity vector, pressure and turbulence parameters. The turbulence parameters were obtained using the standard k-ε model [14]. The governing equations are given by :

Continuity equation:

$$\frac{\partial}{\partial x}(\rho u) + \frac{1}{r}\frac{\partial}{\partial r}(\rho v r) = 0 \qquad (1)$$

x- momentum equation:

$$\frac{\partial}{\partial x}(\rho u^2) + \frac{1}{r}\frac{\partial}{\partial r}(\rho v r u) - \frac{\partial}{\partial x}(\mu\frac{\partial u}{\partial x}) - \frac{1}{r}\frac{\partial}{\partial r}(r\mu\frac{\partial u}{\partial r}) = -\frac{\partial p}{\partial x} + \frac{\partial}{\partial x}(\mu\frac{\partial u}{\partial x}) + \frac{1}{r}\frac{\partial}{\partial r}(r\mu\frac{\partial v}{\partial r}) \qquad (2)$$

r- momentum equation:

$$\frac{\partial}{\partial x}(\rho u v) + \frac{1}{r}\frac{\partial}{\partial r}(\rho r v^2) - \frac{\partial}{\partial x}(\mu\frac{\partial v}{\partial x}) - \frac{1}{r}\frac{\partial}{\partial r}(r\mu\frac{\partial v}{\partial r}) = -\frac{\partial p}{\partial r} + \frac{\partial}{\partial x}(\mu\frac{\partial u}{\partial r}) + \frac{1}{r}\frac{\partial}{\partial r}(r\mu\frac{\partial v}{\partial r}) - 2\mu\frac{v}{r^2} \qquad (3)$$

k - equation:

$$\frac{\partial}{\partial x}(\rho u k) + \frac{1}{r}\frac{\partial}{\partial r}(\rho v r k) - \frac{\partial}{\partial x}(\frac{\mu}{\sigma_k}\frac{\partial k}{\partial x}) - \frac{1}{r}\frac{\partial}{\partial r}(r\frac{\mu}{\sigma_k}\frac{\partial k}{\partial r}) = G - C_D\rho\varepsilon \qquad (4)$$

ε - equation:

$$\frac{\partial}{\partial x}(\rho u \varepsilon) + \frac{1}{r}\frac{\partial}{\partial r}(\rho v r \varepsilon) - \frac{\partial}{\partial x}(\frac{\mu}{\sigma_\varepsilon}\frac{\partial \varepsilon}{\partial x}) - \frac{1}{r}\frac{\partial}{\partial r}(r\frac{\mu}{\sigma_\varepsilon}\frac{\partial \varepsilon}{\partial r}) = \frac{\varepsilon}{k}(C_1 G - C_2\rho\varepsilon) \qquad (5)$$

where G and μ are the generation term and the effective viscosity respectively, given by

$$G = \mu\left\{2\left[(\frac{\partial u}{\partial x})^2 + (\frac{\partial v}{\partial r})^2 + (\frac{v}{r})^2\right] + \left[\frac{\partial u}{\partial r} + \frac{\partial v}{\partial x}\right]^2\right\} \qquad (6)$$

$$\mu = \mu_\ell + \mu_t \qquad (7)$$

and μ_t is the turbulent viscosity given by

$$\mu_t = \rho C_\mu k^2/\varepsilon \qquad (8)$$

The values of the empirical constants (C_μ, C_1, C_2, σ_k, σ_ε and C_D) used in this study are taken from Reference 14 and are given in Table 1.

Table 1 Empirical constant in k-ε model

C_μ	C_1	C_2	σ_k	σ_ε	C_D
0.09	1.44	1.92	1.0	1.3	1.0

The set of partial differential equations governing the flow examined herein are compactly represented by the following elliptic partial differential equation [14], and the accompanying Table 2 which lists dependent variables and the associated definitions of Γ_ϕ and S_ϕ:

$$\frac{\partial}{\partial x}(\rho u\phi - \Gamma_\phi\frac{\partial\phi}{\partial x}) + \frac{1}{r}\frac{\partial}{\partial r}(\rho r v\phi - \Gamma_\phi r\frac{\partial\phi}{\partial x}) = S_\phi \qquad (9)$$

Table 2 The form of the source terms in the general equation (Equation 9)

ϕ	Γ_ϕ	S_ϕ
1	0	0
u	μ	$-\frac{\partial p}{\partial x} + S^u$
v	μ	$-\frac{\partial p}{\partial r} - \frac{2\mu v}{r^2} + S^v$
k	μ/σ_k	$G - C_D\rho\varepsilon$
ε	μ/σ_ε	$(C_1 G\varepsilon - C_2\rho\varepsilon^2)/k$

The fluxes for the source term S_ϕ are given in Table 2, where certain quantities are defined as follows:

$$S^u = \frac{\partial}{\partial x}(\mu\frac{\partial u}{\partial x}) + \frac{1}{r}\frac{\partial}{\partial r}(r\mu\frac{\partial v}{\partial x}) \qquad (10)$$

$$S^v = \frac{\partial}{\partial x}(\mu\frac{\partial u}{\partial r}) + \frac{1}{r}\frac{\partial}{\partial r}(r\mu\frac{\partial v}{\partial r}) \qquad (11)$$

where, u and v are the axial and radial velocities, respectively. ϕ is the general dependent variable. x and r are the axial

and radial coordinates. ρ and Γ_ϕ are the density and the effective diffusivity coefficients. S_ϕ is the source of ϕ. In the present calculations, equations were solved for continuity and with dependent variables, ϕ, corresponding to the axial and radial velocity components. The effective diffusivity was calculated from the two-equations k- ε turbulence model.

Equations 1 to 5 in their general form of Equation 9 were integrated over the two-dimensional control volume which is created by the staggered grid system to provide the finite difference equations. The discretization scheme used is a hybrid system (an upwind-central difference scheme) explained in detail by Launder and Spalding [14]. The set of the resulting algebraic finite difference equations were solved numerically by an iterative, line-by-line procedure. The present solution method employed the SIMPLE algorithm [15] and upwind differential scheme. The solution procedure used for this flow is embodied in the computer program " TEACH " developed at Imperial College, London. Most of computations were made with a grid of 30×24 nodes with more nodes concentrated near the walls and in regions of separation and high velocity gradients. A grid independence test was conducted, which showed that an increase in the number of nodes from 24×16 to 30×24 modifies the velocity at any particular section of the valve by less than 0.5 % of the maximum velocity at this section. The solution was considered to be converged when the maxima of the mass flux and momentum flux residuals summed at all nodes were less than 0.5 % of the inlet flux.

Flow Configuration and Boundary Conditions

A diagram of the disc valve is shown in Figure 1-a and the solution domain along with the grid used is shown in Figure 1-b. To obtain a solution independent of the number and spacing of the grid nodes, grid sensitively test were performed. The flow computations were performed for different dimensionless valve lifts (H), ranging between 0.05 to 0.36. In addition, the computations were conducted for different dimensionless overlap length of the valve disc (Z) of 0.07, 0.12 and 0.16, and for different dimensionless disc thickness, T = 0.04, 0.08 and 0.12. The dimensionless thickness of the valve seat (T_s) is taken of 0.1 with an orifice opening (β) of 0.48. The governing equations require boundary conditions on all sides of the solution domain shown in Figure 1-b. The inlet boundary condition is located at xu=0.5D upstream of the valve and the outlet is located sufficiently far downstream (xd=14D). At the inlet plane, a fully developed profile of axial velocity and zero radial velocity are assumed. The inlet profile for k and ε are estimated from,

$$k = \alpha U_{in}^2 \quad , \varepsilon = k^{3/2} C_\mu / \ell \qquad (12)$$

where α = 0.03 is estimated from the experimental data, and ℓ is the length scale of turbulence, ℓ = 0.03 R , where R is the pipe radius . No-slip boundary conditions are imposed on the mean velocities at all solid walls, and the streamwise gradient of all unknown variables presented in Table 2 are assumed to vanish at the exit plane. Near the wall, the coutte flow assumption of constant shear stress is made. The wall functions corresponding to the dependent variables which were tested extensively for separation flows are the same as described by Habib and Whitelaw [16] and Habib *et. al.* [17]. At the centerline, the zero-gradient boundary conditions were applied.

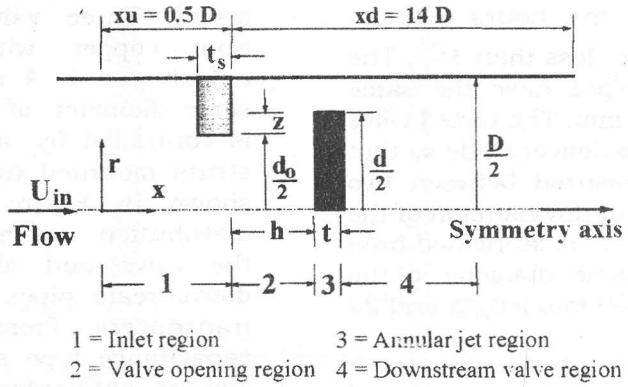

(a)

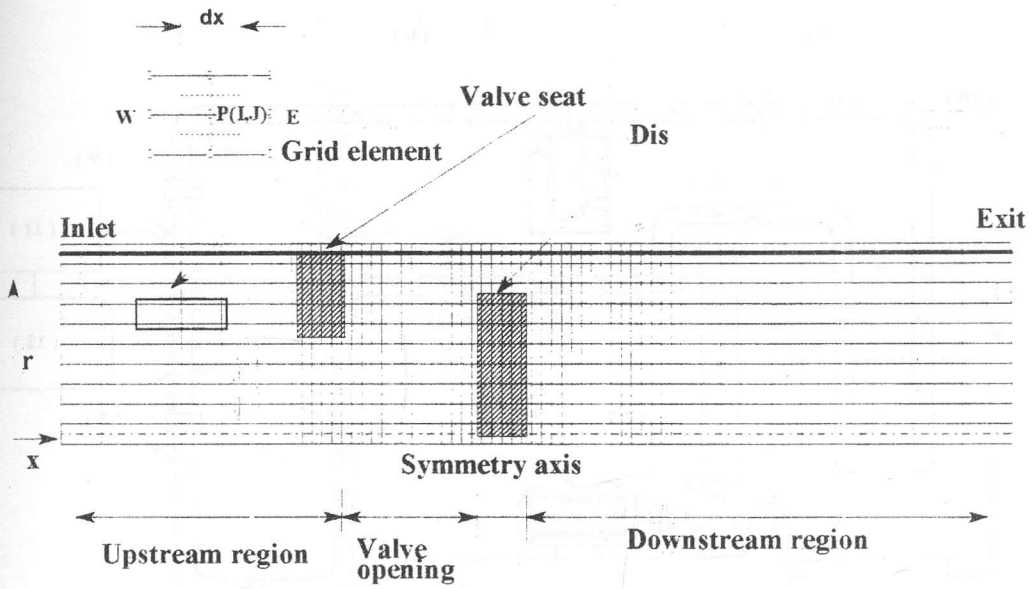

(b)

Figure 1 (a) Disc valve assembly; (b) Grid generation

EXPERIMENTAL SETUP AND MEASUREMENTS DEVICES

A general arrangement of the experimen-tal setup is shown in Figure 2. The closed loop hydraulic circuit consists of a main supply water tank (3), a centrifugal pump (2) and piping system, the test section (7) and a gate valve (4) for controlling the flow rate of water through the hydraulic circuit. A centrifugal pump (2) driven by a 4 HP and 1410 rpm electric motor (1) was used to pump the water from the main supply tank to the test section (7) through the piping system. On leaving the test section, the fluid flow rate through the delivery pipe (10) was measured using a calibrated orifice-meter (5) by a mercury U-tube differential manometer (6). The fluid then flows to the main supply tank

through the control valve. The dimensions of the supply tank allowed a continuous work of the pump up to five hours with an increase of temperature less than $3\,C^{\circ}$. The suction and delivery pipes have the same inner diameter of 100 mm. The tested valve is located on the pump delivery side so that the pressure was measured between two flanges of upstream and downstream of the test section. The section is fabricated from perspix and has the same diameter of the delivery pipe 50 mm, 800 mm length and 22 pressure tapping holes.

A schematic diagram of the non-return valve assembly is shown in Figure 3. For all tests reported in this work, the valve seat diameter (d_o) is 24 mm with 5 mm thickness and the diameter of the downstream pipe (D) is 50 mm. Flat-faced disc valves were tested. Three valve discs were fabricated from copper with different thicknesses, namely t = 2, 4 and 6 mm, and having the same diameter of 35 mm. The valve opening is controlled by a spring which is hold with struts mounted upstream the valve seat, as shown in Figure 3. The static pressure distribution was measured before and after the valve and along the upstream and downstream pipes with the aid of pressure transducers. Pressure transducers with a capacitance type are connected to channel storage oscilloscope where pressure traces are recorded. The pressure transducers are attached to a data acquisition system.

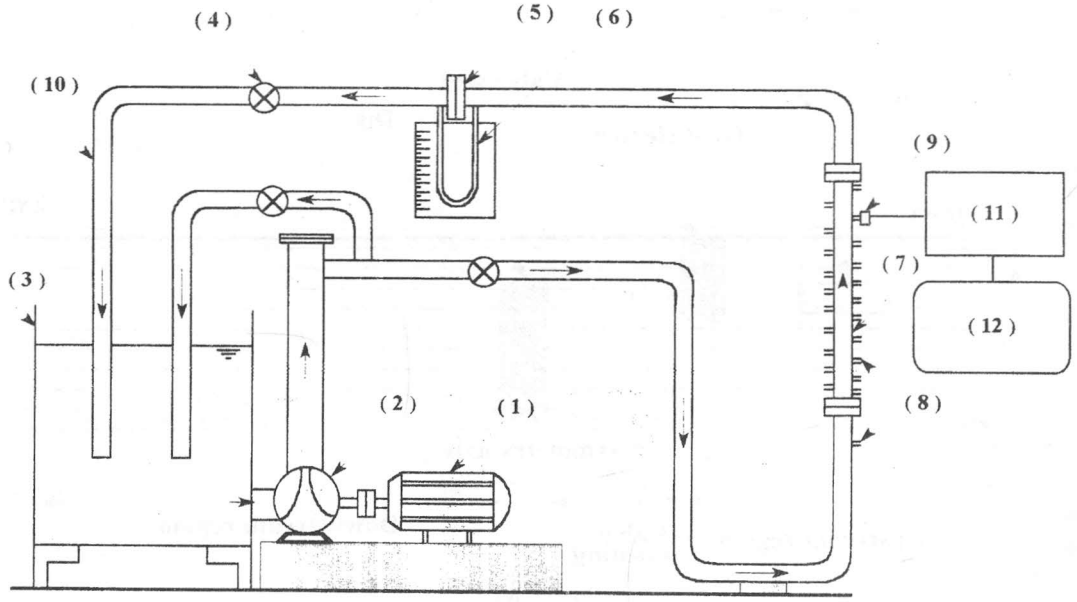

(1) A-C Motor
(2) Centrifugal pump
(3) Supply tank
(4) Control gate valve
(5) Orifice flow meter
(6) Mercury U-Tube differential manometer
(7) Test section
(8) Pressure tapping holes
(9) Pressure transducer
(10) Delivery pipe line
(11) Oscilloscope
(12) Data acquisition system

Figure 2 Schematic layout of the experimental test rig

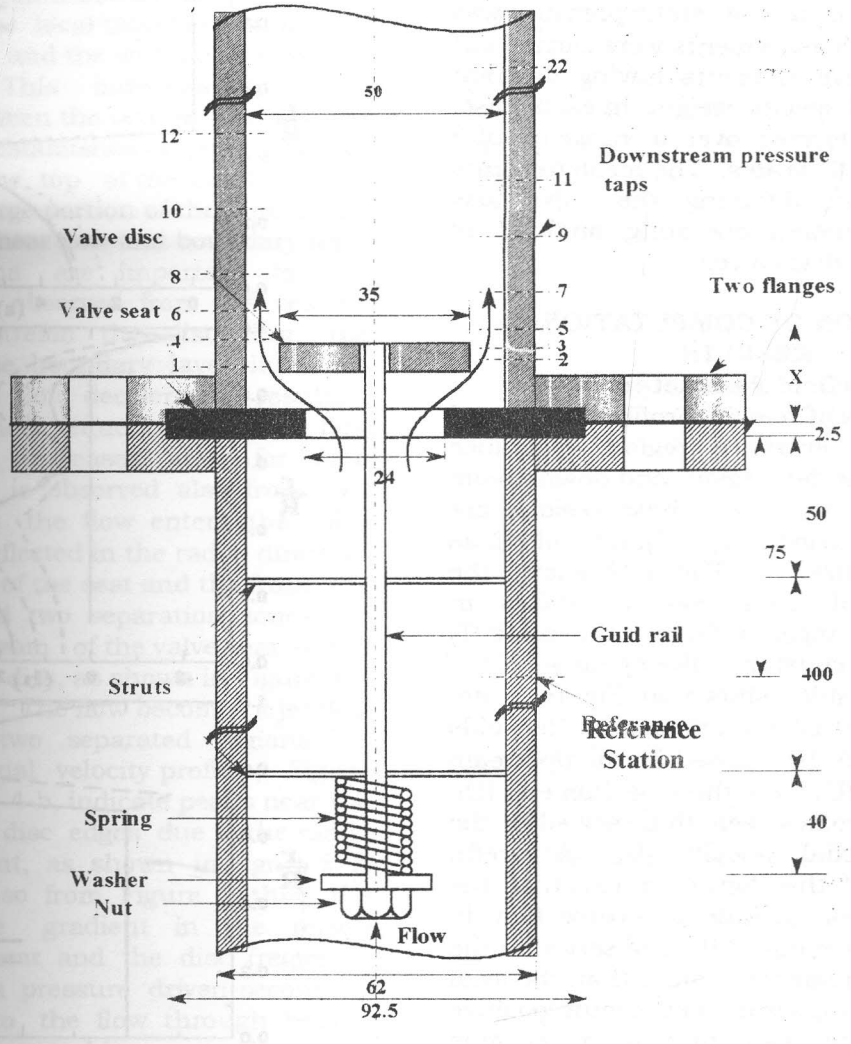

Point No.	1	2	3	4	5	6	7	8	9	10	11
$\overline{X}$	0.32	0.38	0.44	0.50	0.56	0.66	0.78	0.86	1.06	1.26	1.46
Point No.	12	13	14	15	16	17	18	19	20	21	22
$\overline{X}$	1.86	2.26	2.86	3.46	4.26	5.26	6.26	8.26	10.26	12.26	14.26

Figure 3 Non-return disc valve assembly, (dimensions in mm).

The system permits pressure readings for all points at the same time. The experimental error in measuring the static pressure was about ±1%. Measurements were carried out for moving valve elements having different thickness and specific weight. In each case, tests were performed over a range of valve openings and flowrates. The measurements were used for obtaining the valve loss coefficient at different operating conditions of the non-return disc valves.

DISCUSSION OF COMPUTATIONAL RESULTS

Predicted Flowfield Parameters

The results of velocity profiles are plotted in the valve entrance region, clearance region, annular jet region and downstream region behind the disc. These regions are designated as region (1), (2), (3) and (4), as shown in Figure 1-a. Figure 4 shows the distribution of axial velocity profiles in different valve regions for disc thickness (T) of 0.04, and at constant valve opening (H) of 0.08. The results shown in Figure 4 are plotted for Z = 0.12 and at constant Reynolds number of 6.25×10^4 , based on the upstream inlet velocity (U_{in}) and the pipe diameter (D). The velocity profiles seem to be scaled by the inlet mean axial velocity (U_{in}). A careful examination of this figure reveals that, the velocity profiles include a reverse flow in region-2 and region-4. It is observed in the region downstream the valve that, the local axial velocity drops from a maximum positive value near the wall to a negative value behind the valve disc, indicating a central recirculation zone. The recirculation zone occupies along a portion of the pipe cross-section area and maintains a significant presence until a short distance before the downstream pipe exit. The profiles downstream the disc clearly demonstrate that the edge of the wall boundary layer is the location where the axial velocity maximizes.

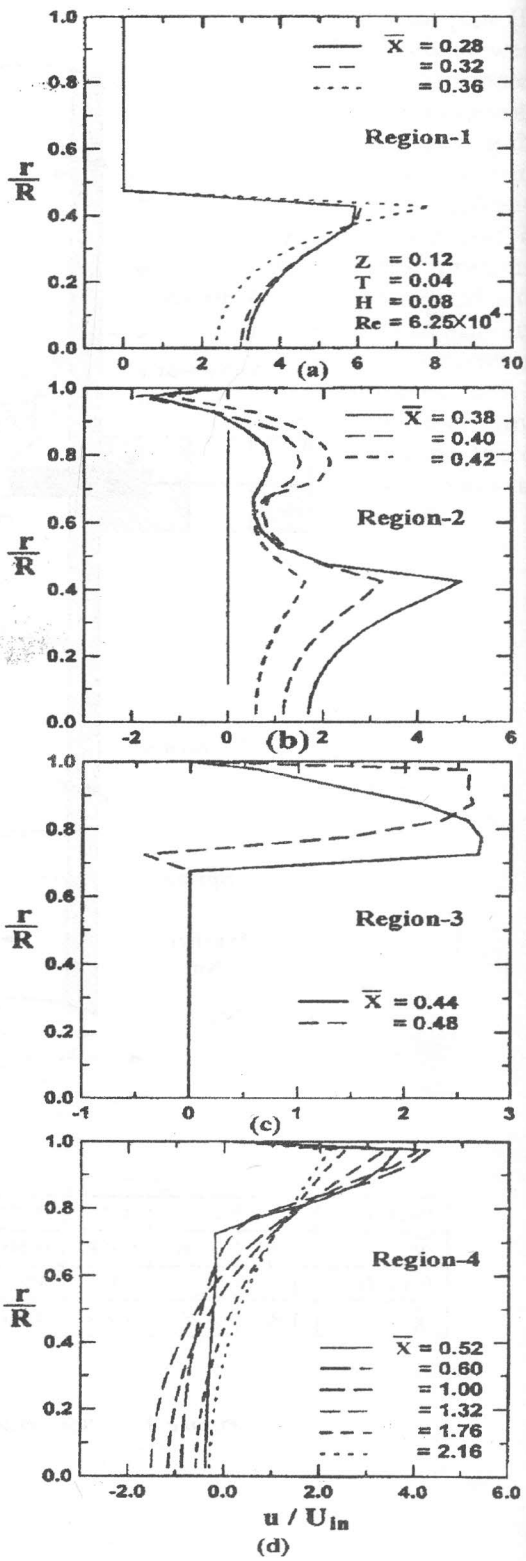

Figure 4 Axial velocity profiles in valve regions, (T_s=0.1 and β=0.48).

Along the axial direction, the axial velocity decays continuously while its profile changes with the local thickness of the wall boundary layer and the width of the reverse flow region. This indicates that the interaction between the reverse flow and the main stream establishes a region of free shear flow at the top of the wall boundary layer over a large portion of the pipe. Thus, both the free shear flow and boundary layer flow phenomena are important to this flowfield. It is observed from the velocity profiles downstream the disc that, the thickness of the boundary layer increases slightly due to flow deceleration resulting from a rapid width reduction of reverse flow region and an increased area for main stream flow. It is observed also from this figure that, as the flow enters the valve region, it is deflected in the radial direction by the rear wall of the seat and the front face of the disc and two separation zones are formed downstream of the valve seat and at the top of valve disc, as shown in Figure 4-b and Figure 4-c. The flow becomes a jet flow bounded by two separated regions. In addition, the axial velocity profiles, Figure 4-a and Figure 4-b, indicate peaks near the valve seat and disc edges due to the radial pressure gradient, as shown in Figure 5. It can be seen also from Figure 5 that, the radial pressure gradient in the region between the seat and the disc (region-2) could create a pressure driven-secondary cells, similar to the flow through bends, which building central jets cause secondary peaks in the axial velocity profiles. In turn, positive radial velocity profiles in the valve regions are observed due to the flow entertainment into the cells, as shown in Figure 6. This effect still found up to the valve exit plane ($\overline{X}$ = 0.6) due to the formation of a wake behind the valve disc.

The distributions of turbulence kinetic energy are presented in Figure 7 at different locations in the valve regions and for the same previous tested conditions. The main observation which can be drawn from this figure is that, the turbulence intensity profiles are consistent with those of the axial velocity profiles, (Figure 4). As expected high values of turbulence intensity are associated with steep mean velocity gradient and with the distortion profiles. The turbulence energy increases steeply in the valve opening and downstream regions due to the high velocity gradients across the separated flow behind the valve seat and the recirculation zone behind the valve disc. The above indicates that a major portion of the flow turbulence is produced by the sharp streamline curvature and the continuous variation of the cross-sectional area create steep pressure gradients of both signs at the seat and valve corners.

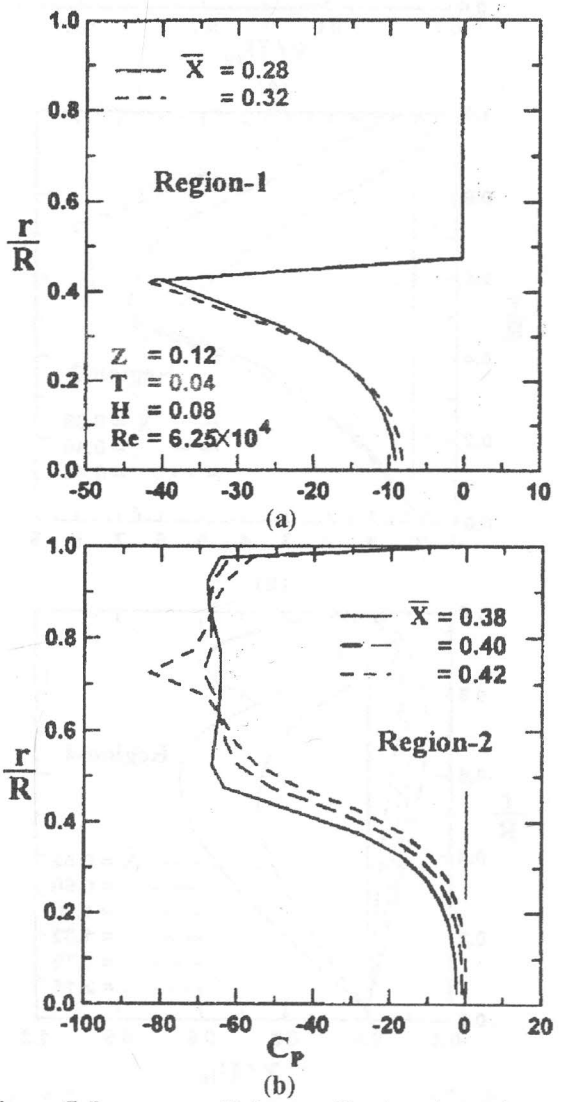

Figure 5 Pressure coefficient profiles in valve regions, (T_s =0.1 and β=0.48)

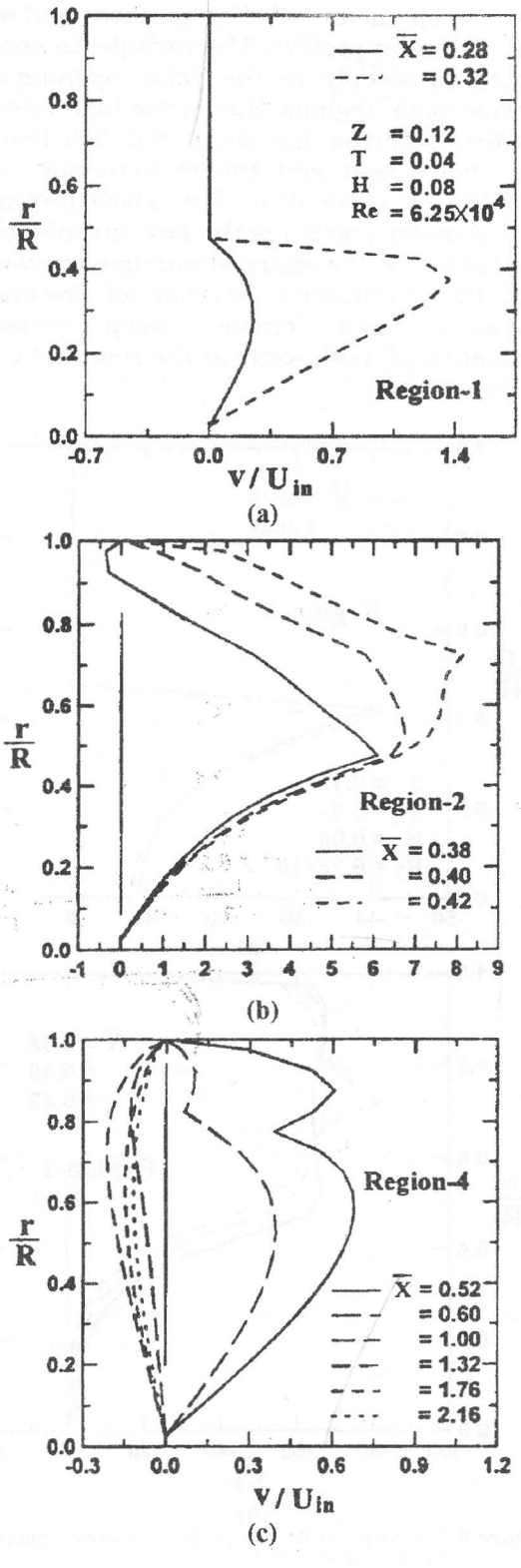

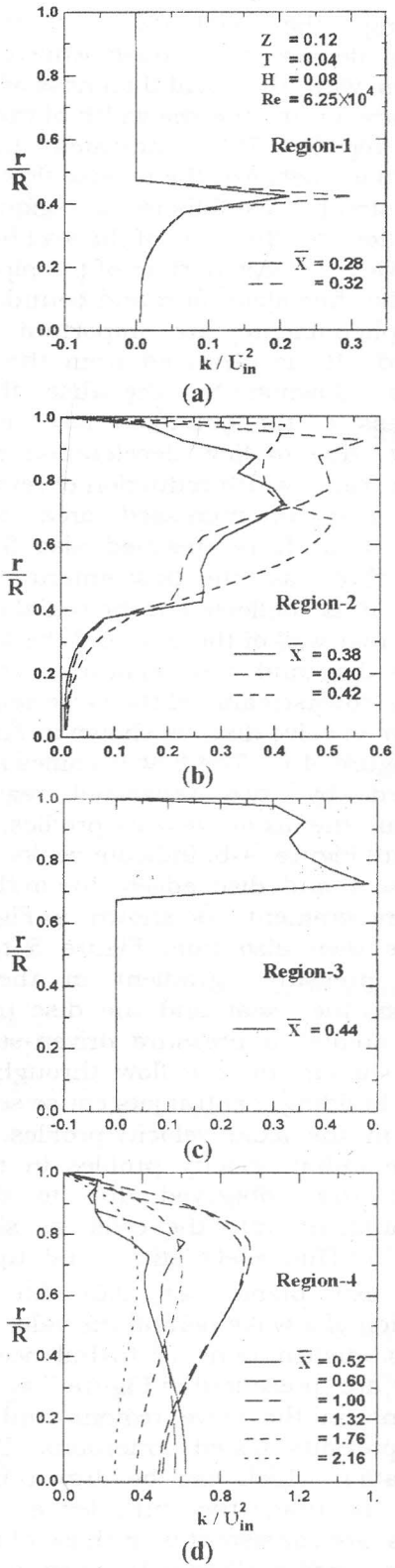

Figure 6 Radial velocity profiles in valve regions, (T_s=0.1 and β=0.48)

Figure 7 Kinetic energy profiles in valve regions, (T_s=0.1 and β=0.48)

Effect of Disc Thickness on Downstream Flow Parameters

The effect of disc thickness on the axial velocity profiles downstream the valve are shown in Figure 8 at $\overline{X}$ = 0.60, 0.68, 1.76 and 2.76, and at constant valve opening namely H = 0.08 and Re = 6.25×10^4. It can be seen from this figure that, the size of recirculation zone downstream the disc decreases with increasing the disc thickness. It is also shown from the figure that the velocity profiles crossover and formed a single profile at $\overline{X}$ = 1.76 and the recirculation zone disappeared completely approximately before $\overline{X}$ = 2.76. The main reason for shrinking the recirculation zone downstream the valve with increasing the disc thickness is that, increasing the disc thickness causes the flow between the disc and the pipe wall (region-2) approaches to the jet flow or flow through a long orifice. In turn, the streamline spread more with increasing the disc thickness and hence, the rate of flow entertainment into the recirculation zone increases. Consequently, the velocity after jet region increases as shown in Figure 8 at $\overline{X}$ = 0.6. This behavior of axial velocity profiles in the recirculation zone is reflected on the distribution of radial velocity profiles, as shown in Figure 9. It is clearly observed from this figure that, the values of radial velocities changes from positive values immediately behind the disc to negative values far downstream the disc. On the other hand, increasing the disc thickness causes an increase in the values of radial velocities, which leads to an increase in the rate of flow entertainment into the recirculation zone generated behind the valve disc. Therefore, it can be concluded that, the majority of the flow going downstream the valve may be loosely described as a turbulent jet surrounded by a pipe wall boundary layer and a recirculation flow region. Thus the flow can be decomposed into three parts: the recirculation flow region, the main jet stream and the wall boundary layer.

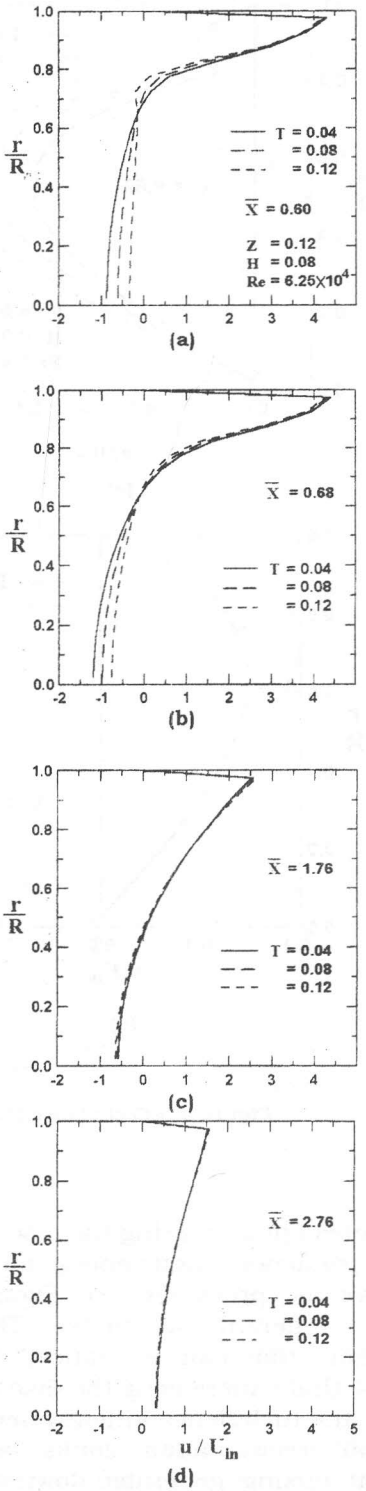

Figure 8 Effect of disc thickness on axial velocity profiles, (T_s=0.1 and β=0.48)

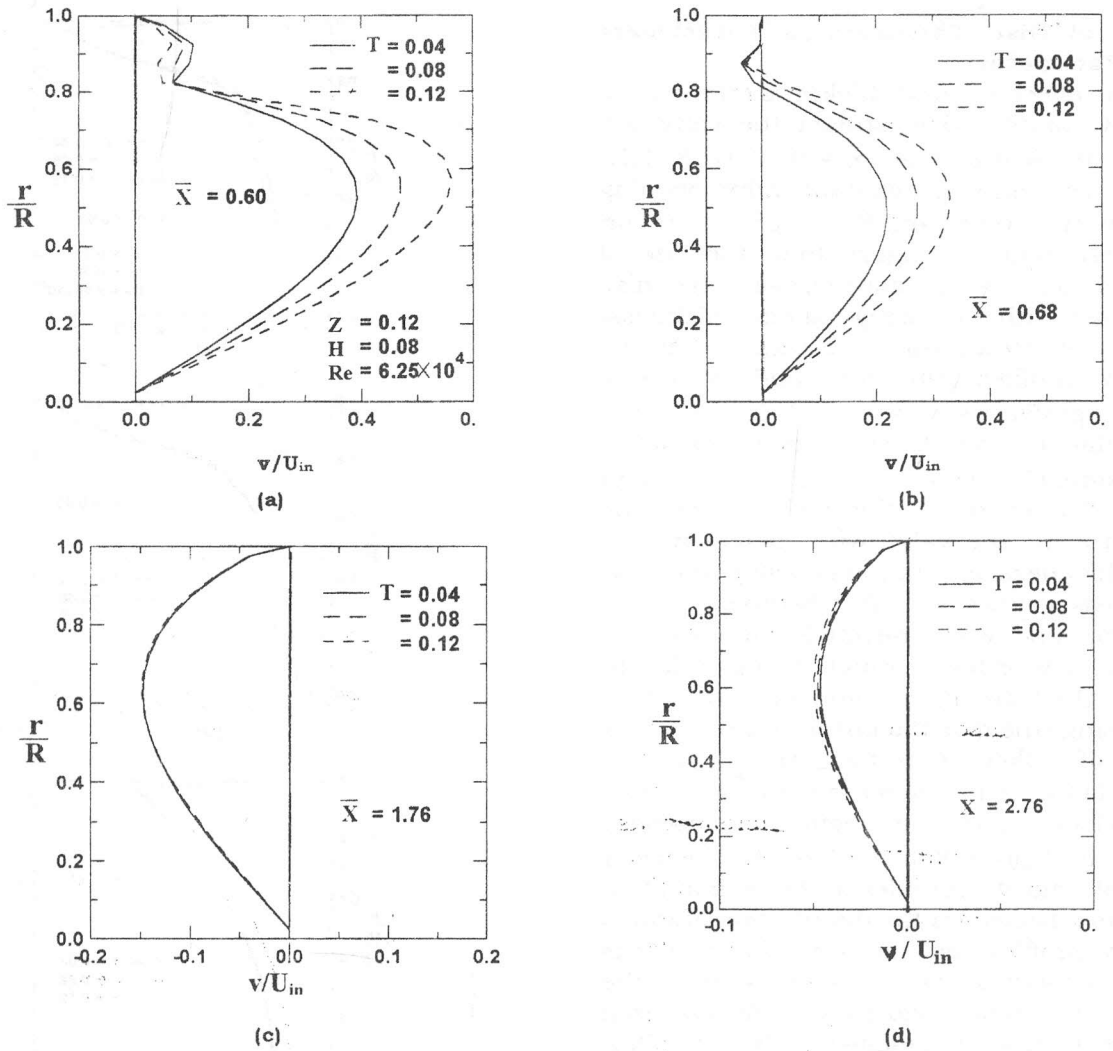

Figure 9 Effect of disc thickness on radial velocity profiles, (T_s = 0.1 and β = 0.48).

The effect of increasing the disc thickness on the turbulence kinetic energy downstream the valve is presented in Figure 10 at selected different locations. The main observation that can be noticed from this figure is that, increasing the disc thickness reduces the turbulence kinetic energy due to the small recirculation zones and small turbulent mixing generated downstream the valve disc. It can be observed also from this figure that, the kinetic energy profiles have main and secondary peaks due to the presence of rear disc edge. These peaks are enlarged as the flow moves in the downstream direction up to $\overline{X}$ = 1.32 and then decayed afterwards. This occurs due to the reduction in the size of recirculation zone.

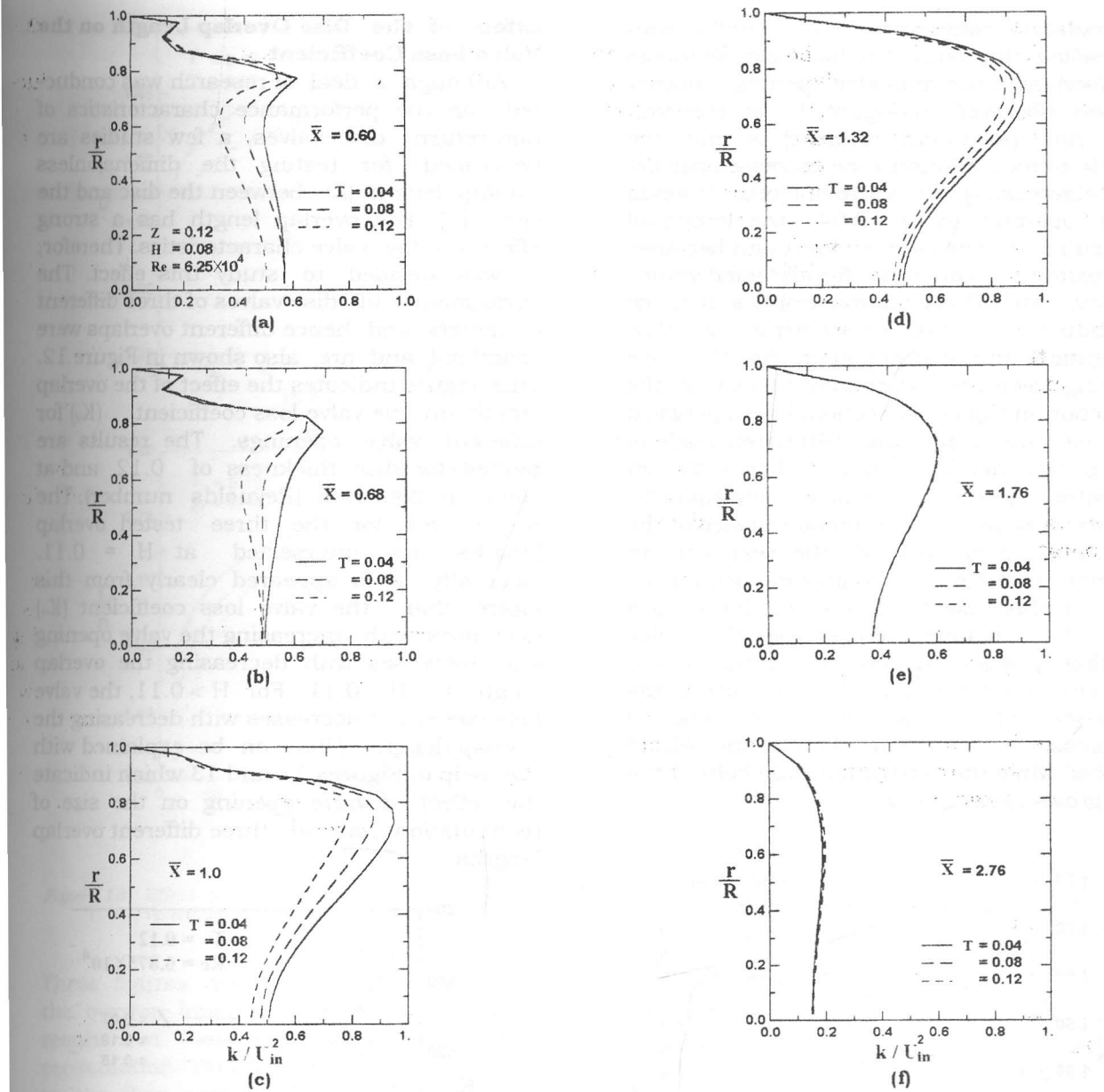

Figure 10 Effect of disc thickness on kinetic energy profiles in streamwise direction, (T_s = 0.1 and β = 0.48).

Effect of Valve Opening on The Recirculation Zone

The performance of check valves such as non-return valves and relief valves are sensitive to the valve geometry as well as operating conditions. It is required that, the flow resistance through the valve to be as low as possible. The loss coefficient of such valves is strongly dependent on the valve opening (H) and flow rate (Reynolds number). The variation of volumatric flow rate is represented herein by the variation of upstream Reynolds number, where the upstream pipe diameter and the fluid properties of the water, such as density and viscosity, are constant. The results of the length of recirculation zone versus flow rate (upstream Reynolds number) are plotted in Figure 11 at five different valve openings. It appears from this figure that, the size of the

recirculation zone increases gradually with increasing the volumetric flow rate (Reynolds number) at constant valve opening. Another feature observed in Figure 11 at constant flow rate (Reynolds number) is that, the length of recirculation zone increases rapidly with decreasing the valve opening. At small valve opening (H = 0.04), the length of recirculation zone is maximized and becomes approximately constant for all tested values of flow rate. These characteristics may be attributed to the phenomena of flow separation and reattachment. As the valve opening decreases at constant flow rate, the reduction in the cross-sectional area between the seat and valve disc ultimately leads to higher flow acceleration and hence steeper pressure gradient, which consequently results in substantial reduction in size of the separation zone behind the seat and an increase in the recirculation zone behind the disc. In this case, the flow through the valve may be cavitates. Increasing the valve opening results in flow deceleration and pressure recovery due to increasing the cross-sectional area, which causing a suppression of the recirculation zone behind the disc while the separation zone behind the seat grows again in size.

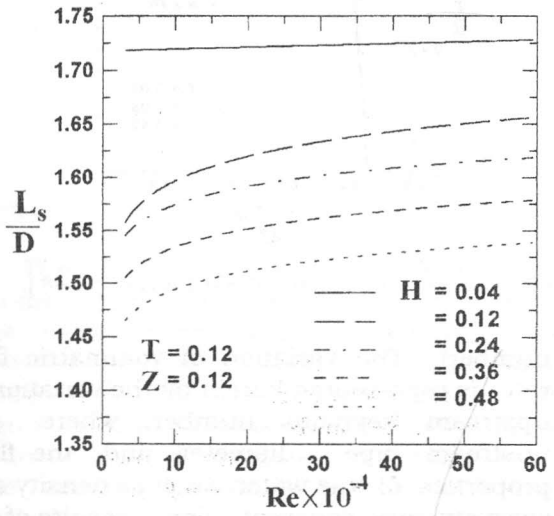

Figure 11 Effect of valve opening on the size of recirculation zone, (T_s = 0.1 and β = 0.48).

Effect of the Disc Overlap Length on the Valve Loss Coefficient

Although a deal of research was conducted on the performance characteristics of non-return disc valves, a few studies are performed for testing the dimensionless overlap length (Z) between the disc and the seat [7]. The overlap length has a strong effect on the valve characteristics. Therefor, it was decided to study this effect. The performance of disc valves of three different diameters and hence different overlaps were examined and are also shown in Figure 12. This figure indicates the effect of the overlap length on the valve loss coefficient (K_v) for different valve openings. The results are plotted for disc thickness of 0.12 and at constant flow rate (Reynolds number). The K_v– curves for the three tested overlap lengths are intersected at H = 0.11. Generally, it is appeared clearly from this figure that, the valve loss coefficient (K_v) decreases with increasing the valve opening and increases with decreasing the overlap length for H< 0.11. For H > 0.11, the valve loss coefficient decreases with decreasing the overlap length. This can be explained with the help of Figures 11 and 13 which indicate the effect of valve opening on the size of recirculation zone at three different overlap lengths.

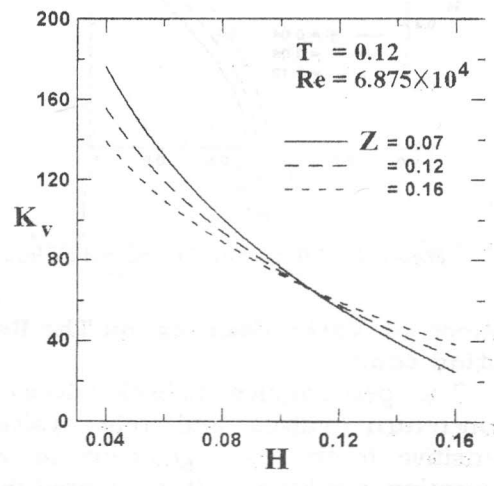

Figure 12 Effect of disc overlap on valve loss coefficient, (T_s = 0.1 and β = 0.48).

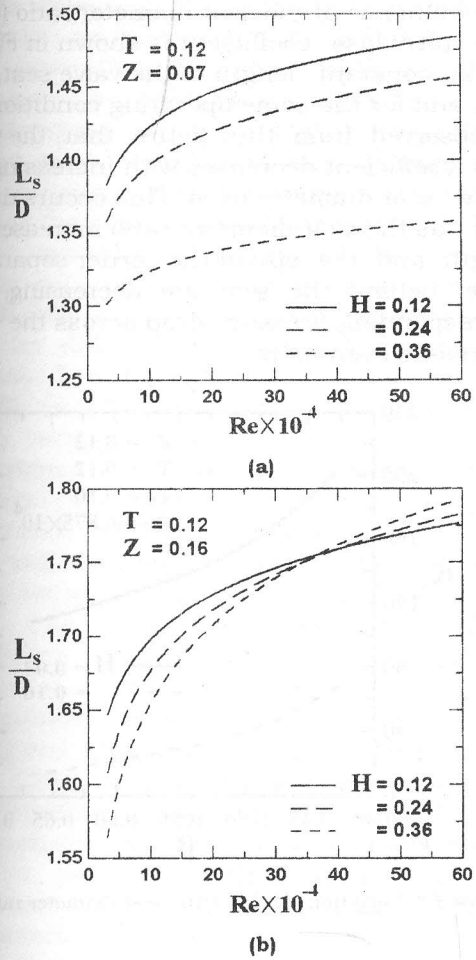

Figure 13 Effect of disc overlap on the size of recirculation zone, (T_s = 0.1 and β = 0.48).

These figures demonstrate that, increasing the overlap length at constant valve opening results in an increase of the size of recirculation zone behind the valve disc, due to the flow acceleration in jet region, and consequently a reduction in the separation zone behind the seat. On the other hand, for Z = 0.07 and 0.12, Figure 13-a and Figure 11 respectively, increasing the valve opening causes a reduction of the recirculation zone and an increase in the size of separation zone behind the seat. For Z = 0.16, the trend is reversed where the size of recirculation zone increases with increasing the valve opening. Therefor, the valve loss coefficient strongly depends on the overlap length in addition to valve opening, as shown in Figure 14. Since the valve loss coefficient is generally decreases with increasing the valve opening. At small valve opening, the valve loss coefficient decreases with increasing the overlap length when the flow rate was kept constant through the valve. At large openings, K_v becomes smaller and increases slightly with increasing the overlap length. These characteristics can be attributed to the phenomena of flow separation and reattachment and the pressure recovery downstream of the valve disc.

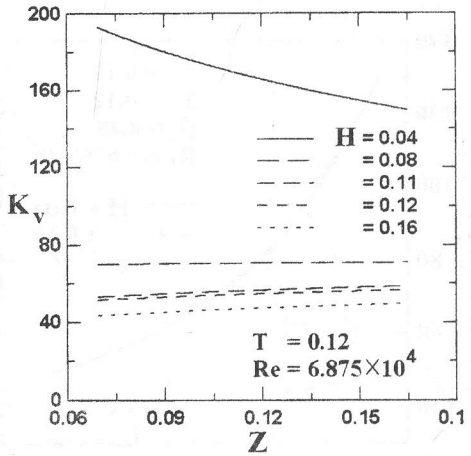

Figure 14 Variation of valve loss coefficient with disc overlap for different valve opening, (T_s = 0.1 and β = 0.48).

Effect of Seat Geometry on Valve Loss Coefficient

The effect of changing the length of the valve seat (T_s) on the valve loss coefficient (K_v) is presented in Figure 15 for two values of valve opening H = 0.04 and 0.16 and at constant flow rate. The results are plotted for seat diameter ratio of β = 0.48 and dimensionless disc thickness of T = 0.12. It appears from this figure that, increasing the length of valve seat at constant seat diameter ratio decreases the valve loss coefficient due to a reduction of the pressure drop across the valve as shown in Figure 16 which represents a sample of predicted wall pressure distribution in the streamwise direction. It appears also that the rate of decrease of the valve loss coefficient at small valve opening is higher than that for the large valve opening. The wall pressure distribution which is shown in Figure 16, indicates that, the pressure drops before the

valve seat and then there is a high pressure drop within the valve seat region due to the acceleration of the fluid. In the valve opening region, some pressure recovery is obtained due to increasing the effective flow area and again the pressure drops in the jet and recirculation regions. At the end of the recirculation zone behind the valve disc, the flow is reattached to the pipe wall and after some pressure recovery it adjusts again to the linear drop of a fully developed pipe flow.

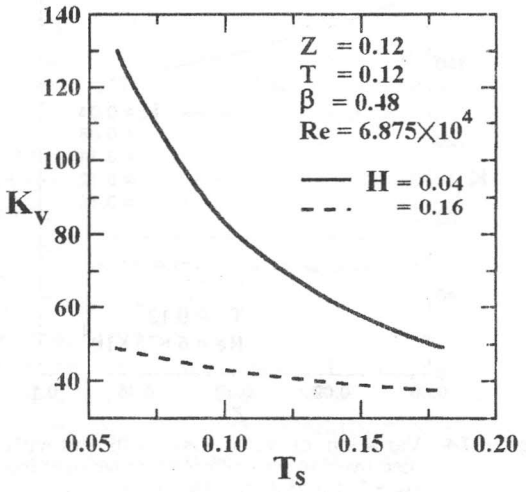

Figure 15 Effect of the valve seat length on valve loss coefficient

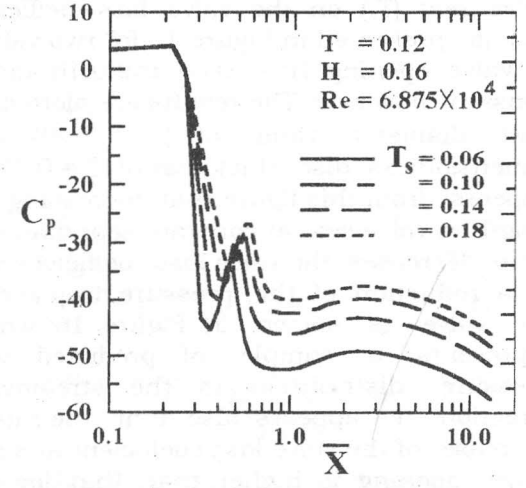

Figure 16 Effect of the valve seat length on the wall pressure coefficient

The influence of the seat diameter ratio (β) on the valve loss coefficient is shown in Figure 17 at constant length of the valve seat, T_s = C.1, and for the same operating conditions. It is observed from this figure that, the valve loss coefficient decreases with increasing the valve seat diameter ratio. This occurs due to that, as the seat diameter ratio increases the length and the size of the corner separation zone behind the seat are decreasing. The corresponding pressure drop across the valve decreases even more.

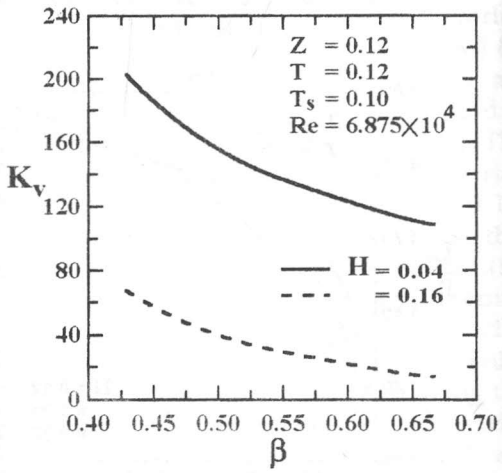

Figure 17 Variation of K_v with seat diameter ratio (β).

COMPARISON WITH EXPERIMENTAL RESULTS

To verify the present computational technique with the measured data, a series of computation were performed on disc valves. The measured inlet velocity (U_{in}) and the valve opening (H) are used in the computations as inlet conditions with specified geometry of pipe, valve seat and disc. The results were compared with experimental measurements in the form of pressure coefficient (C_p), which is defined as $(P - P_{ref})/(0.5\,\rho\,U_{in}^2)$, and valve loss coefficient (K_v), which is defined as the pressure drop across the valve divided by the dynamic pressure. The meshes were designed to give maximum concentration of cells in the valve region, while avoiding excessive distortion of individual cells. Upstream and downstream

of the valve seat, the density of the mesh was reduced as the gradient of the flow variables are generally less and the flow in these regions is of lesser interest. This arrangement ensures maximum accuracy with good computational efficiency. By consideration of the simulated pressure drop across the valve, the valve loss coefficient (K_v) was calculated. Comparisons between measured and computed results of pressure coefficient at constant valve opening of 0.6 and for different thickness of moving disc, namely T = 0.04, 0.08 and 0.12, are shown in Figure 18. It is noticed from this figure that, correlation between computation and experiment is good. However, some differences between the measured and computed results of pressure coefficient in the wake behind the disc and the separation zone between the valve seat and the moving disc. The predicted values of valve loss coefficient (K_v) for disc valve with different thickness, obtained from a series of computation with different valve opening, are compared with experimental values in Figure 19. Good correlation between experiment and prediction was observed. The difference between the experimental and computational results increases with increasing the disc thickness. This may be explained as follows. In general, these results can be taken as an indication that the commonly available turbulence models, such as the k-ε model, may give unreliable prediction where the flow separation and reattachment are occured. Further inaccuracies in the prediction of flow separation and reattachment will be caused by the use of logarithmic wall functions. In addition, numerical inaccuracy can be caused by neglecting the effect of streamline curvature in the separation and recirculation regions.

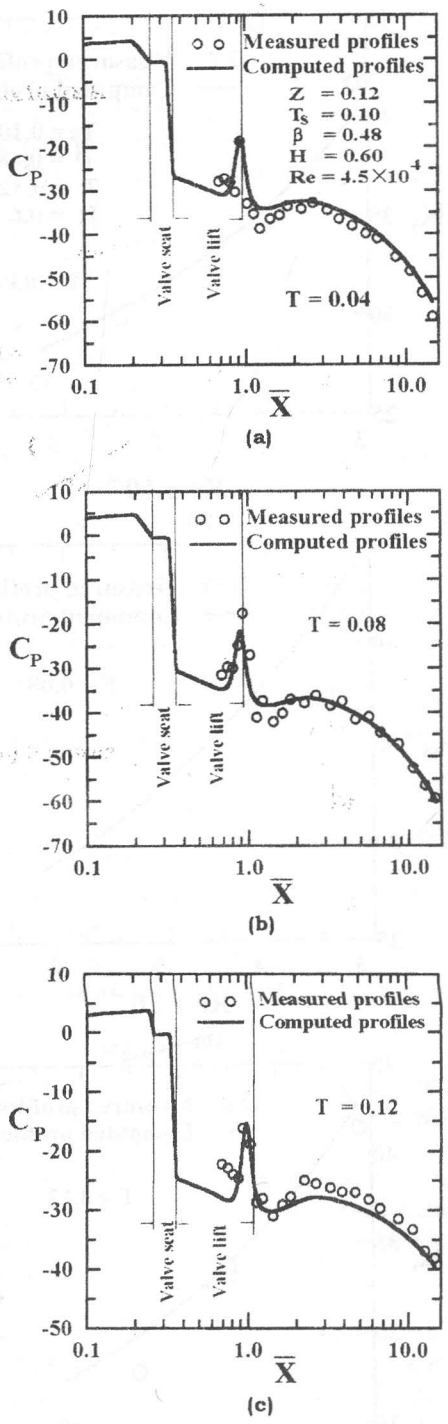

Figure 18 Comparison between predicted and measured C_p

فحص السريان الإضطرابى فى صمامات اللارجوع القرصية

حسن عوض عبد الله، بسيونى أحمد خليفة، أحمد سليمان حزين،
أحمد رأفت دياب و سامية نصر الدين عبده
قسم هندسة القوى الميكانيكية – كلية الهندسة – شبين الكوم – جامعة المنوفية

ملخص البحث :

يتناول هذا البحث بالدراسة النظرية السريان الإضطرابى الغير قابل للإنضغاط خلال صمامات اللارجوع القرصية. تم وضع المعادلات الحاكمة للسريان، كما استخدم معادلات النموذج الإضطرابى لحساب اللزوجة الإضطرابية. وبحل هذه المعادلات أمكن توقع وتقييم سلوك وخصائص السريان خلال هذا النوع من الصمامات، وكذلك أمكن توقع حساب المفاقيد فى الصمام. أجريت الحسابات النظرية عند فتحات مختلفة للصمام، وكذلك تم دراسة العوامل الهندسية للصمام مثل : سمك القرص – الطول التراكبى بين القرص وقاعدة الصمام – سمك قاعدة الصمام ، لبيان تأثير ذلك على مفاقيد الصمام وسلوك السريان خلاله.

لتحقيق النموذج الرياضى للدراسة النظرية، تم تصنيع صمام قرصى لارجوعى ووضع بين أنبوب أمامى وأنبوب خلفى مصنوعتان من البرسبكس ولهما نفس القطر، وكذلك تم تصنيع ثلاثة أقراص للصمام بسمك مختلف. تم أخذ النتائج المعملية لتوزيع الضغط قبل وخلال وبعد الصمام بإستخدام حساسات للضغط وأمكن حساب معامل الفقد خلال الصمام بمعرفة الإنخفاض فى الضغط خلاله. أجريت التجارب المعملية عند معدلات تصرف مختلفة خلال الصمام.

أظهرت النتائج النظرية لتوزيع السرعات وجود إنفصال للسريان خلف قاعدة الصمام وعند حافة القرص، كذلك ظهور منطقة دوامية خلف قرص الصمام، حيث ينعكس ذلك على توزيع الضغط الإستاتيكى خلال الصمام. أوضح توزيع السرعة خلف الصمام أنه يمكن تقسيم السريان إلى ثلاثة أنواع : سريان نفاث – سريان خلال الطبقة المتاخمة – سريان دوامى، والتداخل بين الأنواع الثلاثة للسريان يزيد من صعوبة دراسة وتحليل هذا النوع من السريان. كذلك بينت الدراسة النظرية أن طول وحجم المنطقة الدوامية يزيد مع زيادة رقم الرينولدز ويقل مع زيادة فتحة الصمام. كذلك يقل طول المنطقة الدوامية مع زيادة سمك قرص الصمام. أظهرت النتائج النظرية أن معامل الفقد خلال الصمام يزيد مع زيادة الطول التراكبى بين القرص وقاعدة الصمام حتى فتحة صمام أقل من ١١,. من قطر أنبوب الصمام، ومع زيادة فتحة الصمام بعد ذلك يقل معامل الفقد. تمت مقارنة النتائج المعملية لتوزيع الضغط ومعامل الفقد خلال الصمام مع النتائج النظرية المأخوذة من النموذج الرياضى لهذا البحث، ولقد أظهرت هذه المقارنة تقاربا معقولا بين كل من النتائج النظرية والقياسات المعملي